

Theoretical study of the effective modulus of a composite
considering the orientation distribution of the fillers and the
weakened interface

Sangryun Lee¹ and Seunghwa Ryu^{*,1}

Affiliations

¹ Department of Mechanical Engineering, Korea Advanced Institute of Science and
Technology (KAIST), 291 Daehak-ro, Yuseong-gu, Daejeon 305-701, Republic of Korea

* Corresponding author e-mail: ryush@kaist.ac.kr

Keywords

Homogenization; Micromechanics; Orientation average; Weakened interface

Abstract

In the manufacturing process of a filler-reinforced composite, the fillers in the matrix are aligned due to the shear flow occurring during the drawing stage, and the interface between the matrix and the fillers form various imperfections that lead to debonding and slip under mechanical loading. Hence, there have been numerous micromechanics studies to predict effective moduli of the composites in the presence of partial alignment of fillers and interface imperfections. In this study, we present an improved theory that overcomes two limitations in the existing micromechanics based approaches. First, we find that the interface damage tensor, which has been developed to model the weakened interface between matrix and fillers, has singularities that cause non-physical predictions (such as infinite or negative effective moduli). We correct the mathematical mistakes to remove singularities and derive analytic expressions of the damage tensor for ellipsoidal inclusions. Second, we reveal that the previous theory on the effective moduli with axisymmetric filler orientation distribution fails because the longitudinal and transverse moduli do not converge in the limit of random orientation distribution. With appropriate corrections, we derive an analytic expression for the orientation average of arbitrary transversely isotropic 4th order tensor under general axisymmetric orientation distribution. We apply the improved method to compute the effective moduli of a representative composite with non-uniform filler orientation and interface damage.

1. Introduction

Nanocomposites (such as polymer reinforced with carbon nanotubes (CNTs), graphene, and nanowires), which exhibit remarkable mechanical, electrical, and thermal properties compared to the properties of the bare matrix, have attracted considerable attention because of their numerous potential applications, including flexible sensors[1, 2], lithium batteries[3-5], optical device[6, 7], and flexible energy storage devices[8, 9]. To effectively design and make use of the nanocomposites, it is essential to accurately predict the effective properties of the composite as a function of shape, volume fraction, and orientation distribution of fillers.

For example, the piezoresistivity of the metal nanowire-polydimethylsiloxane (PDMS) composites has been utilized for the highly stretchable strain sensors[2]. The effective electrical property of such composites has been analyzed by solving three dimensional electric circuit constructed from a percolation network of thousands of nanowires[1]. For other examples, the finite element method (FEM) was used to compute the effective moduli of composites at the bulk scale[10-12], whereas molecular dynamics (MD) simulations were used at the atomic scale[13-15]. The aforementioned examples require computationally expensive and time-consuming calculations of a large simulation cell involving many fillers for serving as the representative volume element (RVE).

To compute the effective properties more efficiently, many micromechanics-based approaches have been used, such as the Eshelby method, the Mori-Tanaka (MT) method, and the Self-Consistent (SC) method. Eshelby was the first to introduce the Eshelby tensor (S) and to solve the single inhomogeneity in the matrix by converting the problem into an equivalent eigenstrain problem[16]. The S tensor, which is a 4th order tensor that depends on the matrix properties and the shape of fillers, relates the eigenstrain of equivalent inclusion (fillers) and the constrained strain of matrix. As extensions of the approach, the Eshelby method, the MT

method, and the SC method are devised; these methods are mean-field homogenization schemes to treat the multiple inhomogeneity problems[17]. The MT method is the most popular method because it provides more accurate predictions on the effective properties than the Eshelby method and has an explicit and closed-form solution, whereas the SC method relies on implicit equations. However, the original MT method suffers from two limitations: first, it does not account for the imperfections in the filler-matrix interface, such as debonding and slip; second, it is only applicable when the fillers in the matrix are perfectly aligned in one direction.

To take into account the reduced effective modulus from the weakened interface, Qu et al. introduced the interface spring model, which assumes a virtual linear spring at the interface to allow for a displacement jump across the interface[18]. The 4th order interfacial tensor (R tensor) (H tensor in Qu et al.[18]) was defined to represent the degree of interface damage as a function of the filler shape and the compliance of the interface springs. The modified Eshelby tensor is then obtained by using the R tensor, which eventually leads to the change in the effective modulus prediction. Barai et al. first derived the analytic expression of the R tensor for the axisymmetric ellipsoidal fillers[19]. Because the shape of most fillers (such as spherical nanoparticles or carbon nanotube) can be approximated as axisymmetric ellipsoids with varying aspect ratio, the approach has been used to predict the effective moduli of various composites[14, 20, 21]. However, we find that the mathematical errors and the resulting singularity in R tensor have not been recognized and mentioned in the previous studies^{14, 20, 21}.

In addition, in the manufacturing process of filler-reinforced composite fillers, the fillers in the matrix are aligned because of the shear flow during the drawing stage[22-24]. Hence, it is crucial to predict the effective modulus as a function of the filler orientation distribution[25]. Odegard et al. suggested the orientation average of 4th order stiffness tensor

using the 3-1-3 Euler angle and showed that the effective moduli become anisotropic when the fillers are partially or fully aligned[26]. However, we find that their prediction on the effective moduli with axisymmetric filler orientation distribution fails because the longitudinal and transverse moduli do not converge in the limit of random orientation distribution. Meantime, the orientation average scheme has been applied to the study of the effective moduli of composites with various types[15, 27, 28].

In this work, we propose an improved micromechanics model to correct the two problems regarding the interface damage and the orientation average. First, we obtain the analytic expressions by solving the integral form of R tensor analytically for axisymmetric ellipsoidal fillers and validate our results against the numerical integration results. We also confirm that our expression satisfies two limiting cases, i.e., aspect ratio of 1 and infinity, where analytic results are readily available[18]. We demonstrate that the singularities in effective modulus prediction can be removed when the correct R tensor is used. Second, instead of the 3-1-3 Euler angle, we use polar and azimuthal angles on the unit sphere to represent the filler orientation and derive algebraic expressions for the general transversely isotropic 4th order tensor under axisymmetric filler orientation distribution. We confirm that the longitudinal and transverse elastic moduli from our model converge to the moduli of randomly oriented case of which the analytic expression exists[17]. In summary, we derive analytic expressions for the general axisymmetric orientation distribution of axisymmetric ellipsoidal fillers with a damaged interface described by the linear spring model, which can be widely used to describe composites that include particles and fillers at various aspect ratios.

2. Methods

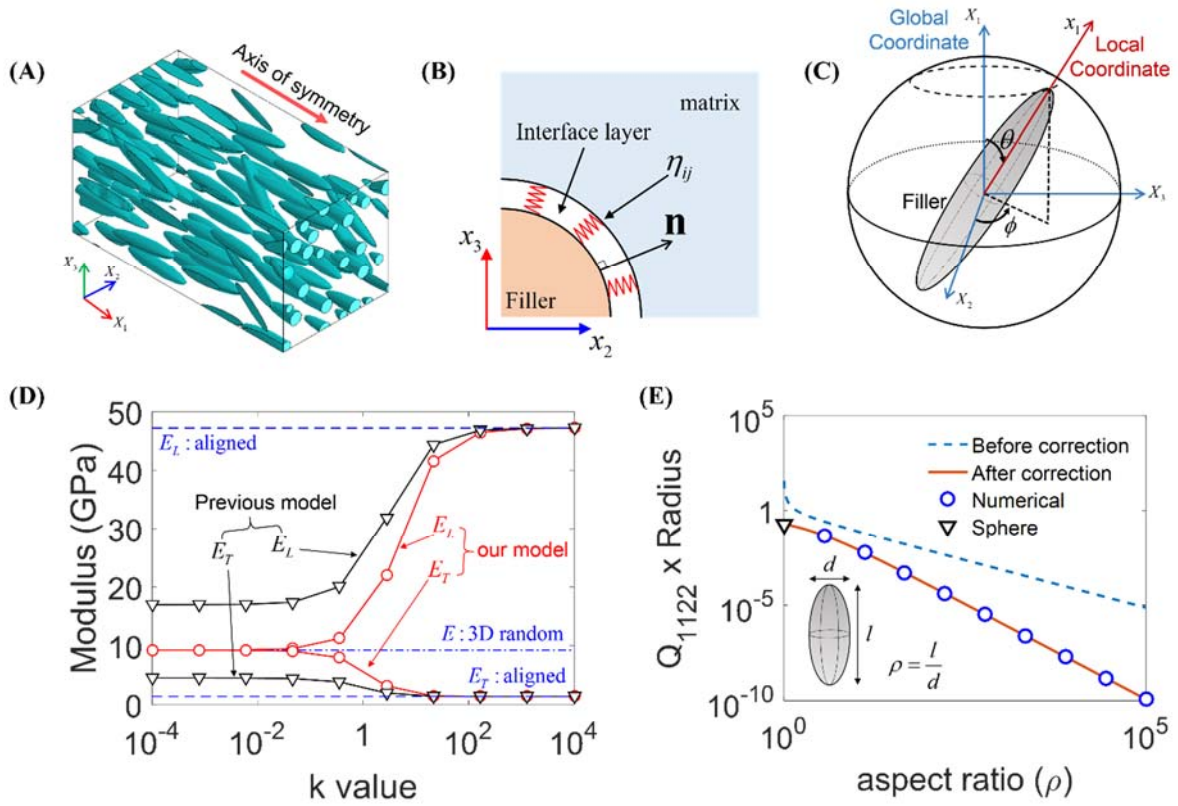


Figure 1 (A) Schematic of RVE with partially aligned fillers. (B) Interface spring model to simulate the damaged interface between matrix and filler. (C) The local coordinates (x_1, x_2, x_3) and global coordinates (X_1, X_2, X_3) displayed with the spherical coordinates. (D) Modulus in the longitudinal and transverse directions. The dashed lines are the results from known analytic expressions. The parameters used in calculation are listed in Table 1 (E) Previous and corrected Q_{1122} component, one of the damaged interface properties components, with respect to the aspect ratio of the filler. The triangular symbol is the known value at the aspect ratio of 1 reported by Qu et al.[18].

We adopt Hill's notation to calculate the effective modulus of RVE, as shown Fig. 1(A). To perform the complex calculations of 4th order tensors, such as double-contraction and

inverse conveniently, we follow the Walpole's scheme[17]. In what follows, the capital sized alphabets represent 4th order tensors, and the colons denote double contraction operations. The effective stiffness tensor of the composite in the original MT approach is expressed as below.

$$L_{eff} = (c_0 L_0 + c_1 L_1 : A) : (c_0 I + c_1 A)^{-1} \quad (1)$$

where L_0 and L_1 are the stiffness tensors of the matrix and filler, respectively. I is the 4th order identity tensor. c_0 and c_1 refer to the volume fraction of matrix and fillers, respectively; thus, $c_0 + c_1 = 1$. A is the strain concentration tensor defined in Eq. (2) and is expressed in terms of Eshelby tensor (S) and stiffness tensors.

$$\varepsilon_1 \equiv A : \varepsilon^{ext}, \quad A = [I + S : L_0^{-1} : (L_1 - L_0)]^{-1}, \quad \varepsilon_0 \equiv S : \varepsilon^* \quad (2)$$

Here, ε^* is the eigenstrain, and ε_0 and ε_1 are the averaged strain values within the matrix and the fillers, respectively. The Eshelby tensor (S) for the filler whose shape is axis-symmetry ellipsoid is taken from Qiu et al.[17].

As mentioned previously, the original MT method is only applicable when the fillers are completely aligned and have perfect bonding with the matrix. The modified Mori-Tanaka (mMT) approach must be employed to account for the imperfect bonding at the interface (slip or debonding). To model the weakened interface bonding, we consider the displacement jump across the interface by adopting the linear spring model[18], given by Eq. (3).

$$\Delta u_i = \eta_{ij} \sigma_{jk} n_k, \quad \eta_{ij} = \alpha \delta_{ij} + (\beta - \alpha) n_i n_j \quad (3)$$

where the η_{ij} tensor refers to the compliance of the interface spring in the tangential (α) and normal (β) directions. After solving the eigenstrain problem with the displacement jump, we obtain the modified Eshelby tensor (\tilde{S}) as follows:

$$\tilde{S} = S + (I - S) : R : L_0 : (I - S). \quad (4)$$

In this work, we limit our focus on the axisymmetric ellipsoidal fillers with two semi-axial lengths of a_1 along the x_1 direction and a along the x_2 and x_3 directions. Due to the nonphysical overlapping arising from a nonzero β , the R tensor is typically expressed by considering only tangential spring compliance as

$$R_{ijkl} = \alpha(P_{ijkl} - Q_{ijkl})$$

where

$$P_{ijkl} = \frac{3}{16\pi} \int_0^\pi \left[\int_0^{2\pi} (\delta_{ik}\hat{n}_j\hat{n}_k + \delta_{jk}\hat{n}_i\hat{n}_l + \delta_{il}\hat{n}_k\hat{n}_j + \delta_{jl}\hat{n}_k\hat{n}_i)n^{-1}d\theta \right] \sin\phi d\phi$$

and

$$Q_{ijkl} = \frac{3}{4\pi} \int_0^\pi \left[\int_0^{2\pi} \hat{n}_i\hat{n}_j\hat{n}_k\hat{n}_l n^{-3}d\theta \right] \sin\phi d\phi.$$

with $\hat{\mathbf{n}} = \left(\frac{\cos\phi}{a_1}, \frac{\sin\phi\cos\theta}{a}, \frac{\sin\phi\sin\theta}{a} \right)^T$, $n = \sqrt{\hat{n}_i\hat{n}_i} = \frac{1}{\rho a} \sqrt{\cos^2\phi + \rho^2 \sin^2\phi}$, and $\rho = \frac{a_1}{a}$.

The non-zero components of P and Q can be obtained from the integral given below:

$$P_{1111} = \frac{3}{2a} \frac{1}{\rho^2 - 1} \left[\frac{\rho^2}{\sqrt{\rho^2 - 1}} \sin^{-1} \frac{\sqrt{\rho^2 - 1}}{\rho} - \frac{1}{\rho} \right], \quad P_{2222} = \frac{3}{2a} \left[\frac{\rho}{\sqrt{\rho^2 - 1}} \frac{\rho^2 - 2}{2(\rho^2 - 1)} \sin^{-1} \frac{\sqrt{\rho^2 - 1}}{\rho} + \frac{\rho}{2(\rho^2 - 1)} \right]$$

$$P_{1212} = \frac{1}{4}(P_{1111} + P_{2222}), \quad P_{2323} = \frac{1}{2}P_{2222}$$

$$Q_{1111} = \frac{3}{2a} \left[\frac{2\rho^2 + 1}{\rho(\rho^2 - 1)^2} - \frac{3\rho}{(\rho^2 - 1)^{5/2}} \sin^{-1} \frac{\sqrt{\rho^2 - 1}}{\rho} \right], \quad Q_{1122} = \frac{3}{4a} \left[\frac{\rho(\rho^2 + 2)}{(\rho^2 - 1)^{5/2}} \sin^{-1} \frac{\sqrt{\rho^2 - 1}}{\rho} + \frac{-3\rho}{(\rho^2 - 1)^2} \right]$$

$$Q_{2222} = \frac{9}{8a} \left[\rho - \frac{\rho^3(2\rho^2 - 5)}{2(\rho^2 - 1)^2} + \frac{\rho^3(\rho^2 - 4)}{2(\rho^2 - 1)^{5/2}} \sin^{-1} \frac{\sqrt{\rho^2 - 1}}{\rho} \right], \quad Q_{2233} = \frac{1}{3}Q_{2222}.$$

Other components can be obtained by using the symmetry condition in the 2-3 plane as well as the minor and major symmetry of P and Q tensors. In the limit of zero spring compliance, the modified Eshelby tensor becomes the original Eshelby tensor because R becomes zero tensor, and hence, mMT method becomes MT method. The effective moduli in the mMT

scheme can be obtained by replacing the original Eshelby tensor S with the modified Eshelby tensor \tilde{S} , as presented below[18]:

$$L_{eff} = (c_0 L_0 + c_1 L_1 : \tilde{A}) : (c_0 I + c_1 \tilde{A} + c_1 R : L_1 : \tilde{A})^{-1} \quad (5)$$

where \tilde{A} is the modified strain concentration tensor, $\tilde{A} = [I + \tilde{S} : L_0^{-1} : (L_1 - L_0)]^{-1}$.

We find that there exists a mathematical error in Q_{1122} component and typographical errors in the Q_{1111} and Q_{2222} components in the previous study[19] and that these errors were applied to the several follow-up studies[14, 19-21]. We plot the Q_{1122} component in terms of the aspect ratio ρ in Fig. 1(E). The uncorrected Q_{1122} diverges as the aspect ratio goes to unity and overestimates the value for the entire range of ρ . Because the R tensor plays a critical role in determining modified Eshelby tensor and effective modulus, we expect that the effective modulus with non-corrected R tensor will have singularities at some values of the aspect ratio. We confirm that the newly obtained analytic expression of Q_{1122} predicts the same result with the numerical integration with Gaussian quadrature. In addition, our expression matches with the readily available analytic expression at two limiting case of $\rho = 1$ and $\rho = \infty$ obtained by Qu et al.[18]. We present the validation of all other nonzero components in Appendix A.

The derived mathematical expression on the effective modulus is only applicable for the composites with completely aligned fillers. However, usually, fillers are randomly oriented or partially aligned in the manufacturing processes[23, 24, 29]. Because the originally randomly oriented fillers in the liquid-state matrix are partially aligned along the drawing axis in most manufacturing processes and experiments, we limit our focus on the axisymmetric orientation distribution. Following the previous studies, we define the orientation averaged Mori-Tanaka (oaMT) as Eq. (6).

$$L_{eff} = (c_0 L_0 + c_1 \langle L_1 : \tilde{A} \rangle) : (c_0 I + c_1 \langle \tilde{A} \rangle + c_1 \langle R : L_1 : \tilde{A} \rangle)^{-1} \quad (6)$$

where the operator $\langle \rangle$ denotes the orientation average of each tensor. When the shape of fillers is an axisymmetric ellipsoid, the orientation average of an arbitrary 4th order tensor X can be defined as

$$\langle X_{ijkl} \rangle = \frac{\int_0^{\frac{\pi}{2}} \int_{-\frac{\pi}{2}}^{\frac{\pi}{2}} X'_{ijkl}(\phi, \theta) \lambda(\theta) \sin(\theta) d\phi d\theta}{\int_0^{\frac{\pi}{2}} \int_{-\frac{\pi}{2}}^{\frac{\pi}{2}} \lambda(\theta) \sin \theta d\phi d\theta} \quad (7)$$

where θ and ϕ are azimuthal and polar angle with respect to the global coordinate (see **Fig. 1(C)**). X' is the tensor transformed to global coordinate system. Following the coordinate transformation rule of 4th order tensor with rotation matrix c , X'_{ijkl} can be expressed as Eq.(8).

$$X'_{ijkl} = c_{ip}c_{jq}c_{kr}c_{ls}X_{pqrs} \quad c = \begin{bmatrix} \cos\theta & -\sin\theta & 0 \\ \sin\theta\cos\phi & \cos\theta\cos\phi & -\sin\phi \\ \sin\theta\sin\phi & \cos\theta\sin\phi & \cos\phi \end{bmatrix} \quad (8)$$

The axisymmetric filler orientation distribution can be expressed as a function of θ only. The axisymmetric orientation distribution function, $\lambda(\theta)$, can be categorized into three types: 3D random, normal distribution, and aligned.

$$\lambda(\theta) = 1 : \text{random}$$

$$\lambda(\theta) = \exp(-k\theta^2) : \text{normal distribution} \quad (9)$$

$$\lambda(\theta) = \delta(\theta) : \text{aligned}$$

When k in the normal distribution goes to zero or infinite, the distribution converges to random or fully aligned distributions, respectively. We note that previously used 3-1-3 Euler angle set cannot describe the axisymmetric distribution along the X_1 axis due to the geometrical constraint, while several studies have adopted the effective modulus from the 3-1-3 Euler angle set to describe the composites with axisymmetric filler orientation distribution[15, 27, 28]. When k goes to zero, i.e., for a random orientation distribution, the composite must

behave as an isotropic material. However, as shown in Fig. 1(D), the longitudinal and transverse Young's modulus from the previous study do not converge to the same value in the random orientation limit. In contrast, the oaMT with our angle set predicts that both longitudinal and transverse moduli approach the modulus of the composite with randomly oriented fillers, whose analytic expression is available.

The evaluation of the orientation average in Eq. (7) is rather difficult because it involves complex transformations of 4th order tensor to global axis. Hence, no analytic expression exists on the orientation average for general axisymmetric distribution, whereas analytic expressions were derived for the two limiting cases of the fully random and fully aligned distributions. To facilitate the use of the oaMT, we derive algebraic expressions of the orientation averaged transverse isotropic 4th order tensor under general axis-symmetry distribution of $\lambda(\theta)$ in Appendix B. The six independent components of orientation averaged 4th order transversely isotropic tensor can be written as linear combinations of eight constants that are easily obtainable via simple numerical integrals. We expect that our orientation average algebraic expression can be widely applicable to the problems, including 4th order tensors.

3. Results and Discussions

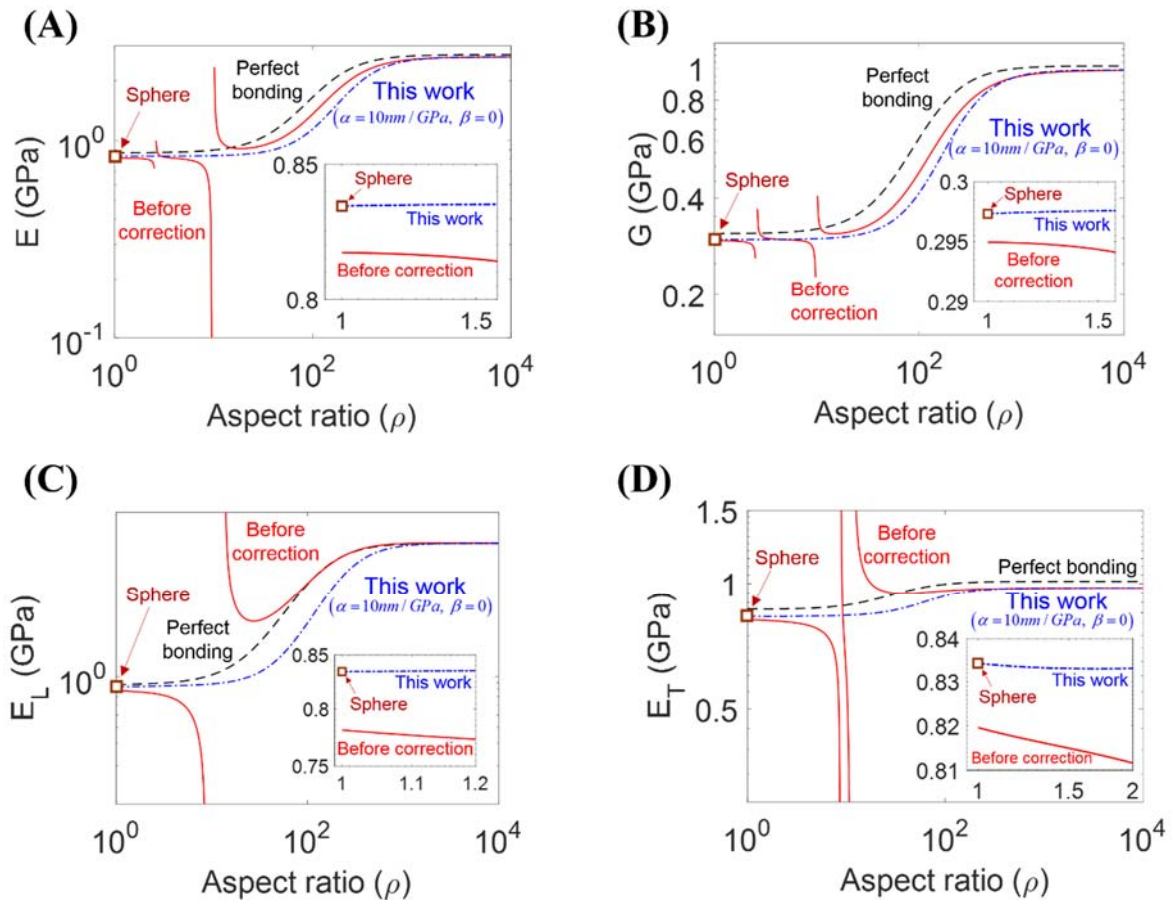


Figure 2 (A) Effective Young's modulus and (B) shear modulus of a composite with randomly oriented fillers. (C) Longitudinal Young's modulus and (D) transverse Young's modulus of a composite whose orientation distribution of fillers is aligned. The insets in each figure show the results near the aspect ratio of 1 to highlight that our model satisfies the limit case with the known analytic expression of spherical fillers. The tangential spring compliance of 10 nm/GPa with zero normal spring compliance is used.

Table 1 Elastic constants used in the calculation of the effective moduli of the CNT-reinforced LaRC-CP2 polymer composite. The data are based on other research studies[19, 26]. The volume fraction of CNT is 0.01 (1%), and the tangential compliance at weakened interface between the polymer and CNT is set 10 nm/GPa[19].

Material properties	Matrix phase	Carbon nanotube (CNT)
Young's modulus (E)	0.85 GPa	
Poisson's ratio (ν)	0.4	
Longitudinal Young's modulus (E_{11})		1.06 TPa
Transverse bulk modulus (κ_{23})		271 GPa
Transverse shear modulus (μ_{23})		17 GPa
In-plane shear modulus (μ_{12})		442 GPa
In-plane Poisson's ratio (ν_{12})		0.162

We apply our new oaMT with the damaged interface to predict the effective moduli of CNT-reinforced LaRC-CP2 polymers. The material constants used in our calculations are listed in Table 1. Following previous studies[19], we only consider the tangential part in the linear spring model (see Fig. 1 (B)) and set the normal compliance to zero ($\beta = 0$) because finite normal spring compliance may cause a nonphysical configuration, such as the overlap of the filler and matrix volumes. To avoid such a problem, it is necessary to set the spring compliance to be a non-linear function of the displacement jump, which makes the evaluation of effective moduli highly difficult[30]. Because this issue is an independent topic in the micromechanics community, we will not consider the normal compliance in our work. Indeed, the tangential spring model is sufficient to model the interfacial slip.

First, we compare the effective moduli of composites with the previous R tensor and the corrected R tensor. We correct two simple typographical errors in the Q_{1111} and Q_{2222}

components, but leave the mathematical error in the Q_{1122} component when considering the previous R tensor. Fig. 2 depicts the elastic moduli as functions of the filler aspect ratio for the two limiting cases of fully random and fully aligned distributions. Figs. 2 (A and B) show the Young's modulus and the shear modulus of the composite when the fillers are randomly oriented. Under perfect interfacial bonding condition, both elastic moduli increase with the aspect ratio of fillers at a given volume fraction (Fig. 2 (A and B)). The moduli dramatically rise when the aspect ratio reaches approximately 100 and saturate when the aspect ratio exceed 1000. The same trend can be found in the longitudinal and transverse Young's modulus in another limit case of fully aligned fillers (Fig. 2 (C and D)). When the interfacial imperfection is taken into account, the effective modulus should become lower than the perfect bonding condition. As shown in the Fig. 2, the effective moduli obtained from the previous R tensor are lower than those with perfect bonding in most of the range. However, they have singularities or negative values at few specific aspect ratios due to the presence of a singularity in the wrongly obtained Q_{1122} component. The singularity in the effective moduli can only be found when the aspect ratio is less than 100, and the number of singularities change with material properties of each phases and the volume fraction of fillers. The insets in Fig. 2 show that effective modulus at the aspect ratio of unity, i.e., $\rho = 1$. The effective moduli based on previous R tensor does not converge to the effective moduli of composite with spherical fillers, i.e., $\rho = 1$, whose analytic expression is available[18]. In comparison, the effective moduli obtained from the corrected R tensor are continuous functions of the aspect ratio, are always lower than the effective moduli with perfect bonding condition, and converge to the known values for spherical fillers. We suspect that these problems have not been identified because previous studies consider the composites having fillers in the range of very high aspect ratio ($> 1,000$) where the previous R tensor does not show a singularity[14, 19-21]. In addition, for large aspect ratio, the difference between the results with previous and corrected R tensors

becomes rather negligible because the Q_{1122} component becomes nearly zero in the limit of large aspect ratio (**Fig. 1(E)**). However, we note that the use of the corrected R tensor is crucial in the small aspect ratio range (< 100).

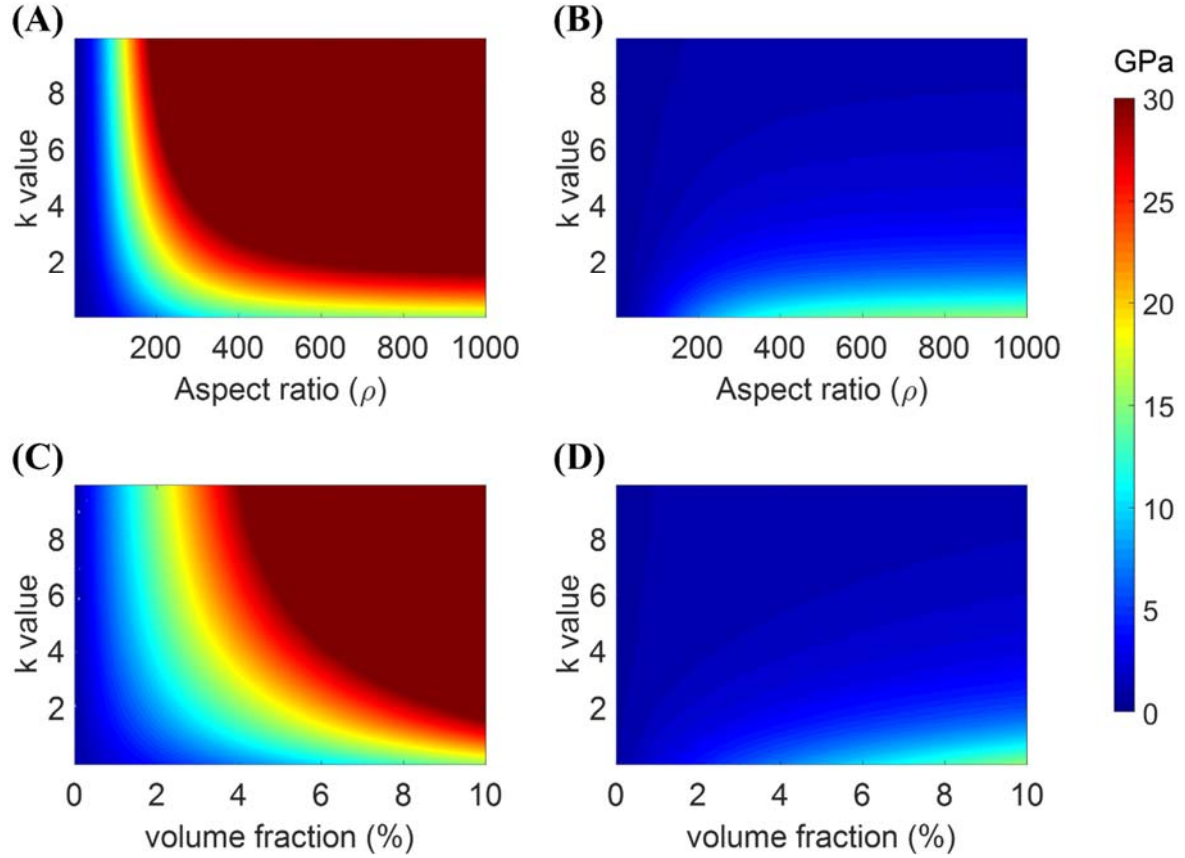


Figure 3 (A) Longitudinal Young's modulus and (B) transverse Young's modulus with a normal distribution of fillers, $\lambda(\theta) = \exp(-k\theta^2)$, as functions of k and aspect ratio under fixed volume fraction (1%). (C) Longitudinal Young's modulus and (D) transverse Young's modulus with respect to the degree of orientation (k) and the volume fraction of the fillers under fixed aspect ratio (1000).

Second, we compute the effective modulus when the fillers are partially aligned with the orientation distribution of $\lambda(\theta) = \exp(-k\theta^2)$. We can study the effect of alignment by

tuning the parameter k . The orientation averaged transversely isotropic tensor in Eq. (6) can be easily evaluated from the linear combinations of eight constants, as described in detail in Appendix B. Figs. 3 (A and B) show the change of longitudinal and transverse Young's modulus with k and aspect ratio ρ at a fixed volume fraction (1%). Because the moduli are calculated from the corrected R tensor, they are free of singularities. When the degree of filler alignment reduces (i.e., when k decreases), the difference between two moduli diminishes and they eventually converges at $k = 0$. We find that both moduli increase with the aspect ratio. In contrast, when k increases, the longitudinal modulus increases whereas the transverse modulus decreases, as expected. We also demonstrate the combined effect of volume fraction and orientation distribution in Figs. 3(C and D). Both moduli increase when the volume fraction increases, and they approach the modulus of matrix in the zero volume fraction limit. We note that the contour plot depicted in Fig. 3 can be easily obtained for any arbitrary axisymmetric orientation distribution of axisymmetric ellipsoidal fillers by computing the eight constants in Appendix B, which will facilitate the use of the micromechanics approach in designing and predicting the performance of the composites.

4. Conclusions

We computed the effective moduli of composites as functions of the aspect ratio of fillers, degree of orientation, and interfacial damage. With appropriate corrections in the previous interfacial damage tensor and orientation average, the spurious singularities in the effective composite modulus predictions are removed, and the longitudinal and transverse moduli converges to a single value as the orientation distribution of fillers becomes random. We demonstrated that the magnitude of moduli can be tuned by either the aspect ratio or the volume fraction and the directional elastic properties can be tuned by controlling the orientation distribution of fillers. To facilitate the application of our method, we derived an analytic expression for the orientation average for arbitrary axisymmetric filler orientation distribution. We believe that our study can provide a comprehensive picture and guidance in the effort to tune the effective moduli of composite materials.

Acknowledgements

This work is supported by the Basic Science Research Program (2013R1A1A1010091) of the National Research Foundation of Korea (NRF), funded by the Ministry of Science, ICT & Future Planning.

Appendix A. Components of weakened interface property tensor, \mathbf{R}

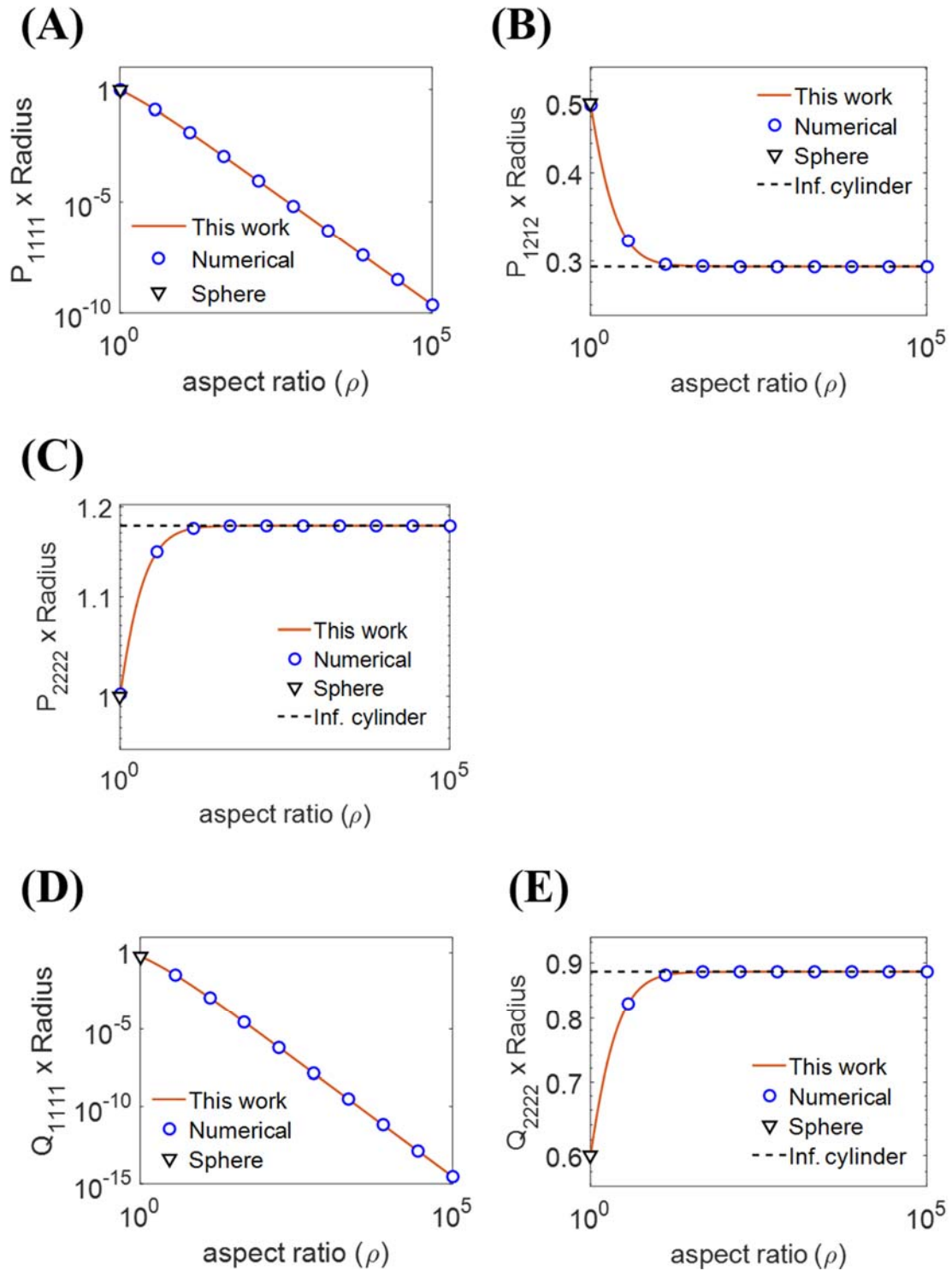


Figure A1 (A) P_{1111} component; (B) P_{1212} component; (C) P_{2222} component; (D) Q_{1111} component;

(E) Q_{2222} component.

Appendix B Orientation average with the rotation matrix

The orientation average of the transversely isotropic 4th order tensor under arbitrary axis-symmetry distribution function, $\lambda(\theta)$, is calculated as

$$A = (2k_0, l_0, l'_0, n_0, 2m_0, 2p_0) \rightarrow \langle A \rangle = (2k_1, l_1, l'_1, n_1, 2m_1, 2p_1)$$

Where the tensors are expressed following Hill's notation for the transversely isotropic 4th order tensor. In the case of the transversely isotropic 4th order material stiffness tensor, the six elastic constants can be determined by following Hooke's law, which is expressed as

$$(\sigma_{22} + \sigma_{33}) = 2k_0(\varepsilon_{22} + \varepsilon_{33}) + 2l'_0\varepsilon_{11},$$

$$\sigma_{11} = l_0(\varepsilon_{22} + \varepsilon_{33}) + n_0\varepsilon_{11},$$

$$(\sigma_{22} - \sigma_{33}) = 2n_0(\varepsilon_{22} - \varepsilon_{33}), \quad \sigma_{23} = 2m_0\varepsilon_{23}$$

$$\sigma_{12} = 2p_0\varepsilon_{12}, \quad \sigma_{13} = 2p_0\varepsilon_{13}$$

The orientation averaged 4th order transversely isotropic tensor, $\langle A \rangle$, can be calculated by using eight constants from numerical integrations.

$$k_1 = \frac{1}{4b_0} [k_0(b_0 + b_1 + 2b_2) + l_0(b_3 + b_4) + l'_0(b_3 + b_4) + m_0(b_0 + b_1 - 2b_2) + n_0(b_5) + p_0(4b_3)]$$

$$l_1 = \frac{1}{2b_0} [k_0(b_3 + b_4) + l_0(b_1 + b_2) + l'_0(b_5) + n_0(b_3) + m_0(b_3 - b_4) + p_0(-4b_3)]$$

$$l'_1 = \frac{1}{2b_0} [k_0(b_3 + b_4) + l(b_5) + l'_0(b_1 + b_2) + n_0(b_3) + m_0(b_3 - b_4) + p_0(-4b_3)]$$

$$n_1 = \frac{1}{b_0} [k_0(b_5) + l_0(b_3) + l'_0(b_3) + n_0(b_1) + m_0(b_5) + p_0(4b_3)]$$

$$m_1 = \frac{1}{8b_0} [k_0(b_0 + b_1 - 2b_2) + l_0(b_3 - b_4) + l'_0(b_3 - b_4) + n_0(b_5) + m_0(b_0 + b_1 + 6b_2) + p_0(4b_3 + 4b_4)]$$

$$p_1 = \frac{1}{16b_0} [k_0(b_0 - b_7) + l_0(-b_0 + b_7) + l'_0(-b_0 + b_7) + n_0(b_0 - b_7) + m_0(5b_0 - 4b_7) + p_0(8b_0 + 4b_7 + 4b_8)]$$

With

$$\begin{aligned}
b_0 &= \int_0^{\frac{\pi}{2}} \lambda(\theta) \sin \theta d\theta, & b_1 &= \int_0^{\frac{\pi}{2}} \lambda(\theta) \cos^4 \theta \sin \theta d\theta, & b_2 &= \int_0^{\frac{\pi}{2}} \lambda(\theta) \cos^2 \theta \sin \theta d\theta \\
b_3 &= \int_0^{\frac{\pi}{2}} \lambda(\theta) \cos^2 \theta \sin^3 \theta d\theta, & b_4 &= \int_0^{\frac{\pi}{2}} \lambda(\theta) \sin^3 \theta d\theta, & b_5 &= \int_0^{\frac{\pi}{2}} \lambda(\theta) \sin^5 \theta d\theta \\
b_6 &= \int_0^{\frac{\pi}{2}} \lambda(\theta) \cos 2\theta d\theta, & b_7 &= \int_0^{\frac{\pi}{2}} \lambda(\theta) \cos 4\theta d\theta
\end{aligned}$$

When $\lambda(\theta)$ is the normal distribution with almost zero k , the orientation average expression in the Appendix reproduces the analytic results of the random orientation case, as already derived in some research studies[14, 17, 19].

References

- [1] Lee S, Amjadi M, Pugno N, Park I, Ryu S. Computational analysis of metallic nanowire-elastomer nanocomposite based strain sensors. *AIP Advances*. 2015;5(11):117233.
- [2] Amjadi M, Pichitpajongkit A, Lee S, Ryu S, Park I. Highly Stretchable and Sensitive Strain Sensor Based on Silver Nanowire–Elastomer Nanocomposite. *ACS Nano*. 2014;8(5):5154-63.
- [3] Cui G, Gu L, Zhi L, Kaskhedikar N, van Aken PA, Müllen K, et al. A Germanium–Carbon Nanocomposite Material for Lithium Batteries. *Advanced Materials*. 2008;20(16):3079-83.
- [4] Huang H, Yin SC, Kerr T, Taylor N, Nazar LF. Nanostructured Composites: A High Capacity, Fast Rate $\text{Li}_3\text{V}_2(\text{PO}_4)_3/\text{Carbon}$ Cathode for Rechargeable Lithium Batteries. *Advanced Materials*. 2002;14(21):1525-8.
- [5] Oh S-M, Oh S-W, Yoon C-S, Scrosati B, Amine K, Sun Y-K. High-Performance Carbon-LiMnPO₄ Nanocomposite Cathode for Lithium Batteries. *Advanced Functional Materials*. 2010;20(19):3260-5.
- [6] Lü C, Cheng Y, Liu Y, Liu F, Yang B. A Facile Route to ZnS–Polymer Nanocomposite Optical Materials with High Nanophase Content via γ -Ray Irradiation Initiated Bulk Polymerization. *Advanced Materials*. 2006;18(9):1188-92.
- [7] Lü C, Guan C, Liu Y, Cheng Y, Yang B. PbS/Polymer Nanocomposite Optical Materials with High Refractive Index. *Chemistry of Materials*. 2005;17(9):2448-54.
- [8] Nyholm L, Nyström G, Mihranyan A, Strømme M. Toward Flexible Polymer and Paper-Based Energy Storage Devices. *Advanced Materials*. 2011;23(33):3751-69.
- [9] Pushparaj VL, Shaijumon MM, Kumar A, Murugesan S, Ci L, Vajtai R, et al. Flexible energy storage devices based on nanocomposite paper. *Proceedings of the National Academy of Sciences*. 2007;104(34):13574-7.
- [10] Banerjee S, Sankar BV. Mechanical properties of hybrid composites using finite element method based micromechanics. *Composites Part B: Engineering*. 2014;58:318-27.
- [11] Sodhani D, Reese S. Finite Element-Based Micromechanical Modeling of Microstructure Morphology in Filler-Reinforced Elastomer. *Macromolecules*. 2014;47(9):3161-9.
- [12] Sun H, Di S, Zhang N, Wu C. Micromechanics of composite materials using multivariable finite element method and homogenization theory. *International Journal of Solids and Structures*. 2001;38(17):3007-20.
- [13] Yang BJ, Shin H, Lee HK, Kim H. A combined molecular dynamics/micromechanics/finite element approach for multiscale constitutive modeling of nanocomposites with interface effects. *Applied Physics Letters*. 2013;103(24):241903.
- [14] Yang S, Yu S, Ryu J, Cho J-M, Kyoung W, Han D-S, et al. Nonlinear multiscale modeling approach to characterize elastoplastic behavior of CNT/polymer nanocomposites considering the interphase and interfacial imperfection. *International Journal of Plasticity*. 2013;41:124-46.
- [15] Alian AR, Kundalwal SI, Meguid SA. Interfacial and mechanical properties of epoxy nanocomposites using different multiscale modeling schemes. *Composite Structures*. 2015;131:545-55.

- [16] Eshelby JD. The Determination of the Elastic Field of an Ellipsoidal Inclusion, and Related Problems. *Proceedings of the Royal Society of London A: Mathematical, Physical and Engineering Sciences*. 1957;241(1226):376-96.
- [17] Qiu YP, Weng GJ. On the application of Mori-Tanaka's theory involving transversely isotropic spheroidal inclusions. *International Journal of Engineering Science*. 1990;28(11):1121-37.
- [18] Qu J. The effect of slightly weakened interfaces on the overall elastic properties of composite materials. *Mechanics of Materials*. 1993;14(4):269-81.
- [19] Barai P, Weng GJ. A theory of plasticity for carbon nanotube reinforced composites. *International Journal of Plasticity*. 2011;27(4):539-59.
- [20] Shokrieh MM, Ghajar R, Shajari AR. The effect of time-dependent slightly weakened interface on the viscoelastic properties of CNT/polymer nanocomposites. *Composite Structures*. 2016;146:122-31.
- [21] Pan Y, Weng GJ, Meguid SA, Bao WS, Zhu ZH, Hamouda AMS. Interface effects on the viscoelastic characteristics of carbon nanotube polymer matrix composites. *Mechanics of Materials*. 2013;58:1-11.
- [22] Fan Z, Advani SG. Characterization of orientation state of carbon nanotubes in shear flow. *Polymer*. 2005;46(14):5232-40.
- [23] Fu SY, Lauke B, Mäder E, Yue CY, Hu X. Tensile properties of short-glass-fiber- and short-carbon-fiber-reinforced polypropylene composites. *Composites Part A: Applied Science and Manufacturing*. 2000;31(10):1117-25.
- [24] Pötschke P, Brüning H, Janke A, Fischer D, Jehnichen D. Orientation of multiwalled carbon nanotubes in composites with polycarbonate by melt spinning. *Polymer*. 2005;46(23):10355-63.
- [25] Buck F, Brylka B, Müller V, Müller T, Weidenmann KA, Hrymak AN, et al. Two-scale structural mechanical modeling of long fiber reinforced thermoplastics. *Composites Science and Technology*. 2015;117:159-67.
- [26] Odegard GM, Gates TS, Wise KE, Park C, Siochi EJ. Constitutive modeling of nanotube-reinforced polymer composites. *Composites Science and Technology*. 2003;63(11):1671-87.
- [27] Pan J, Bian L, Zhao H, Zhao Y. A new micromechanics model and effective elastic modulus of nanotube reinforced composites. *Computational Materials Science*. 2016;113:21-6.
- [28] Nguyen HG, Ortola S, Ghorbel E. Micromechanical modelling of the elastic behaviour of polymer mortars. *European Journal of Environmental and Civil Engineering*. 2013;17(2):65-83.
- [29] Zaixia F, Zhangyu, Yanmo C, Hairu L. Effects of Pre-stretching on the Tensile Properties of Knitted Glass Fiber Fabric Reinforced Polypropylene Composite. *Journal of Thermoplastic Composite Materials*. 2006;19(4):399-411.
- [30] Wang J, Duan HL, Zhang Z, Huang ZP. An anti-interpenetration model and connections between interphase and interface models in particle-reinforced composites. *International Journal of Mechanical Sciences*. 2005;47(4-5):701-18.